Impact Factor : 2.9
Q2

Computational Toxicology 34 (2025) 100354

Contents lists available at ScienceDirect

Computational Toxicology

journal homepage: www.sciencedirect.com/journal/computational-toxicology

Full Length Article

Development of Nipah virus drugs from FDA-approved drugs: An integrated computational approach

Panneerselvam Theivendren [a,*,1], Selvaraj Kunjiappan [b], Parasuraman Pavadai [c], Natarajan Kiruthiga [d], Anusuya Murugavel [e], Avinash Dayalan [e]

[a] Department of Pharmaceutical Chemistry & Analysis, School of Pharmaceutical Sciences, Vels Institute of Science, Technology, & Advanced Studies, Pallavaram, Chennai, Tamil Nadu 600117, India
[b] Department of Biotechnology, Kalasalingam Academy of Research and Education, Krishnankoil 626126 Tamil Nadu, India
[c] Department of Pharmaceutical Chemistry, Faculty of Pharmacy, M.S. Ramaiah University of Applied Sciences, M S R Nagar, Bengaluru 560054 Karnataka, India
[d] Department of Pharmaceutical Chemistry, KMCH College of Pharmacy, Kalappatti Road, Coimbatore 641048 Tamil Nadu, India
[e] Center for Global Health Research, Saveetha Medical College, Saveetha Institute of Medical and Technical Sciences, Chennai 637205 Tamilnadu, India

ARTICLE INFO

Keywords:
Nipah virus
FDA-approved drugs
Molecular docking
Dynamics simulation
Ephrin-B2

ABSTRACT

The Nipah virus (NiV) is a highly virulent zoonotic pathogen that presents a substantial risk to public health, as limited therapeutic interventions are available. The present study utilizes a computational methodology to discover pharmaceutical substances that have been received from the database consisting of 4344 U.S. Food and Drug Administration (FDA)-approved drugs and have the potential to be repurposed to treat NiV infection. We have used molecular docking and dynamics simulation to evaluate the binding affinity and stability of the drugs against the key viral target, Ephrin-B2. The findings of our study demonstrate the presence of numerous FDA-approved drugs that display favourable binding interactions with the target of Ephrin-B2. Within this FDA-approved data set of drugs, we have identified certain FDA-approved drugs, such as Guamecycline, Ergotamine, Sancycline, Entrectinib, and Atogepant, which showed considerably better binding scores. The dynamic behaviour of ligand–protein interaction was evaluated using molecular dynamics simulation, which offered valuable insights into drug-target complexes' temporal stability and conformational alterations. The results of docking studies indicate to active ingredients Guamecycline, Ergotamine, Sancycline, Entrectinib and Atogepant having notable inhibition of the Ephrin-B2 protein. According to the findings from the MD simulation, it was noted that Guamecycline displayed significant interaction with the Ephrin-B2 protein. Therefore, Guamecycline shows potential as a suitable primary chemical for treating NiV. Further, the sub-structures of Guamecycline were used to optimize and substantiate the stability of Guamecycline; in this relation sub, structure **ZINC000169368545** was correlated with Guamecycline, and the observed result showed that the Guamecycline was better lead moiety to inhibit the target Ephrin-B2.

1. Introduction

The ongoing presence of emerging infectious illnesses presents substantial risks to the overall well-being of the global population, and the identification of efficacious treatments for these pathogens continues to be a persistent obstacle [1,2]. Among the several infectious agents, the NiV is notable for its exceptional lethality and concerning pathogenicity, characterized by a high fatality rate, potential for human-to-human transmission, and lack of recognized therapeutic interventions. Since its identification in 1999 during an epidemic in Malaysia, the NiV has been responsible for intermittent outbreaks in South and Southeast Asia, resulting in severe repercussions for the people affected. The prioritization of NiV as a pathogen in urgent need of research and development efforts, particularly in the areas of vaccine development and antiviral therapies, has been undertaken by the World Health Organization (WHO).

NiV is classified within the Paramyxoviridae family and is categorized as a member of the Henipavirus genus, which also encompasses the Hendra virus. Both the NiV and Hendra virus are zoonotic pathogens that exhibit a primary transmission mode from animals to people. These

* Corresponding author.
E-mail address: tpsphc@gmail.com (P. Theivendren).
[1] ORCID: https://orcid.org/0000-0002-8197-4688.

https://doi.org/10.1016/j.comtox.2025.100354
Received 24 July 2024; Received in revised form 13 September 2024; Accepted 5 May 2025
Available online 8 May 2025

viruses are commonly transmitted through contact with fruit bats, which are natural reservoir hosts. These viral pathogens can potentially induce significant respiratory and encephalitic ailments in human hosts, resulting in fatality rates that vary between 40 % and 90 %, contingent upon the specific outbreak and viral strain involved [3,4].

The range of clinical presentations observed in human cases of NiV infection is extensive and frequently includes indications such as elevated body temperature, cranial discomfort, vertigo, and muscular pain. These symptoms may subsequently advance to the development of acute respiratory distress, inflammation of the brain, and convulsions. The transmission of the virus can occur through several means, including proximity to infected animals, ingesting food or beverages that have been contaminated, or human-to-human transmission via respiratory droplets or contact with bodily fluids [5]. The various mechanisms of transmission associated with NiV render it a matter of considerable concern, particularly in settings with low resources where the healthcare system may be insufficient to handle epidemics adequately. There is a lack of authorized vaccinations or targeted antiviral therapies for treating NiV infection. The lack of these preventive approaches presents healthcare providers with restricted choices for controlling epidemics, highlighting the pressing want to advance efficacious treatments. The conventional methods employed for drug discovery and development are characterized by prolonged durations, substantial expenses, and frequent struggles to match the swift advancements in new infectious diseases [6–8].

The utilization of already approved pharmaceutical drugs by the FDA is a viable approach to accelerate the process of discovering and creating new remedies for NiV. Drug repurposing, referred to as drug repositioning or drug reprofiling, is the exploration of established pharmaceutical drugs for potential therapeutic uses that extend beyond their first intended indications. The approach above presents numerous benefits in comparison to the process of de novo drug creation. These advantages encompass shortened timetables for development, decreased costs associated with development, and an increased probability of success owing to the known safety profiles of these medications in human subjects. In light of the urgent demand for medicines targeting NiV, the strategic utilization of FDA-approved drugs is a logical and practical strategy for expeditiously identifying possible therapy options [1,8,9].

Using computational techniques, such as molecular docking and dynamics simulations, has gained significant importance in drug development and repurposing endeavours. These methodologies enable the computational evaluation of the binding affinity and interactions between pharmaceutical compounds and their respective target proteins. Within the framework of NiV, these techniques facilitate the examination of FDA-approved pharmaceutical drugs targeting the essential viral protein Ephrin-B2. This study uses computational methodologies to repurpose medications approved by the FDA to treat NiV infection by evaluating the binding affinity and stability of a collection of 4344 FDA-approved drugs against crucial target Ephrin-B2 of the NiV using molecular docking and dynamics simulations. The findings of this research possess the capacity to identify pharmaceutical candidates with the highest potential for a subsequent preclinical and clinical assessment for drug repurposing. Subsequently, we elucidated the computational methodologies of molecular docking and molecular dynamics simulations, which constitute the fundamental components of our strategy for drug repurposing in the context of NiV [10–13]. The lifecycle of the NiV encompasses several phases, such as viral entry, replication, protein synthesis, and immune evasion. Each of these stages offers promising therapeutic targets for natural bioactive chemicals [14–16]. NiV glycoproteins G and F are crucial components in the process of intracellular entrance. The G glycoprotein allows the virus to bind to receptors on host cells, a process that can be prevented by allicin produced from garlic. On the other hand, the F glycoprotein promotes the fusing of the virus to the cell membrane, a process that is hindered by quercetin found in onion and green tea. Curcumin from turmeric has been demonstrated to suppress the activity of the RNA-dependent RNA polymerase (L), which is crucial for RNA synthesis in viral replication. Likewise, epigallocatechin gallate (EGCG) derived from green tea can interfere with the nucleocapsid protein (N) that encapsulates viral RNA. Resveratrol from grapes can alter the pivotal stage of protein synthesis, in which nonstructural protein P contributes to immune evasion and viral RNA synthesis. Lycopene derived from tomatoes hinders the process of viral assembly by specifically targeting the matrix protein (M). Andrographolide from Andrographis paniculata disrupts host endosomal pathways during viral budding. Furthermore, berberine can effectively modulate immune evasion mechanisms such as the function of nonstructural protein W, while glycyrrhizin derived from liquorice strengthens immunological signalling. The compound baicalin, obtained from *Scutellaria baicalensis*, hinders the activity of viral proteases, therefore causing more disruption to the life cycle of NiV Fig. 1. Our work aims to elucidate the particular NiV protein that was Ephrin-B2 chosen for drug screening and the criteria employed in selecting FDA-approved drugs. Additionally, we will emphasize the importance of our research in addressing the pressing and unfulfilled medical requirement presented by NiV. In conclusion, an outline of the study encompasses a concise summary of the principal parts and their contributions towards the overarching objective of repurposing FDA-approved drugs for treating NiV. This paper aims to elucidate the fundamental ideas, methodology, and computational tools employed in these techniques while examining their practical implementation in drug discovery and repurposing endeavours.

2. Importance of repurposing of FDA-approved drugs for NiV

Outbreaks of the NiV have the potential to escalate rapidly, resulting in substantial morbidity and mortality. The conventional approach to drug development exhibits a need for agility in efficiently addressing emerging risks [17]. Repurposing provides an expedited pathway for identifying prospective therapeutics, facilitating a prompter reaction during epidemics. Creating a novel pharmaceutical compound from its inception necessitates a significant allocation of resources, including large temporal and financial investments. Using alternative purposes leverages prior investments in drug development, leading to cost-effectiveness and optimized allocation of resources. This approach holds particular significance in settings with limited resources. Pharmaceutical products that have received approval from the FDA have already completed extensive safety evaluations in human subjects, mitigating the potential risks associated with unanticipated adverse reactions. The inherent safety profile of these possible NiV therapies facilitates the regulatory approval procedure, hence accelerating their potential availability. This methodology expands the range of therapeutic alternatives by discovering preexisting pharmaceuticals that have antiviral efficacy against NiV. The emergence of drug-resistant strains of NiV over time may necessitate the use of various treatment modalities, making it a crucial consideration. Utilizing molecular docking and dynamics simulations is a contemporary and efficient drug development methodology characterized by its high-throughput nature. The utilization of computer power and advancements in bioinformatics facilitate the in-silico screening of a wide range of potential therapeutic candidates. The aforementioned novel technique is a prime illustration of the convergence of technology and healthcare in tackling rising infectious illnesses. In summary, using repurposing in the context of NiV presents a practical, financially efficient, and scientifically groundbreaking approach to address a highly lethal virus [1]. The intervention can mitigate mortality rates during NiV outbreaks and provide a comprehensive framework for effectively managing other emerging infectious illnesses that require prompt and efficient responses.

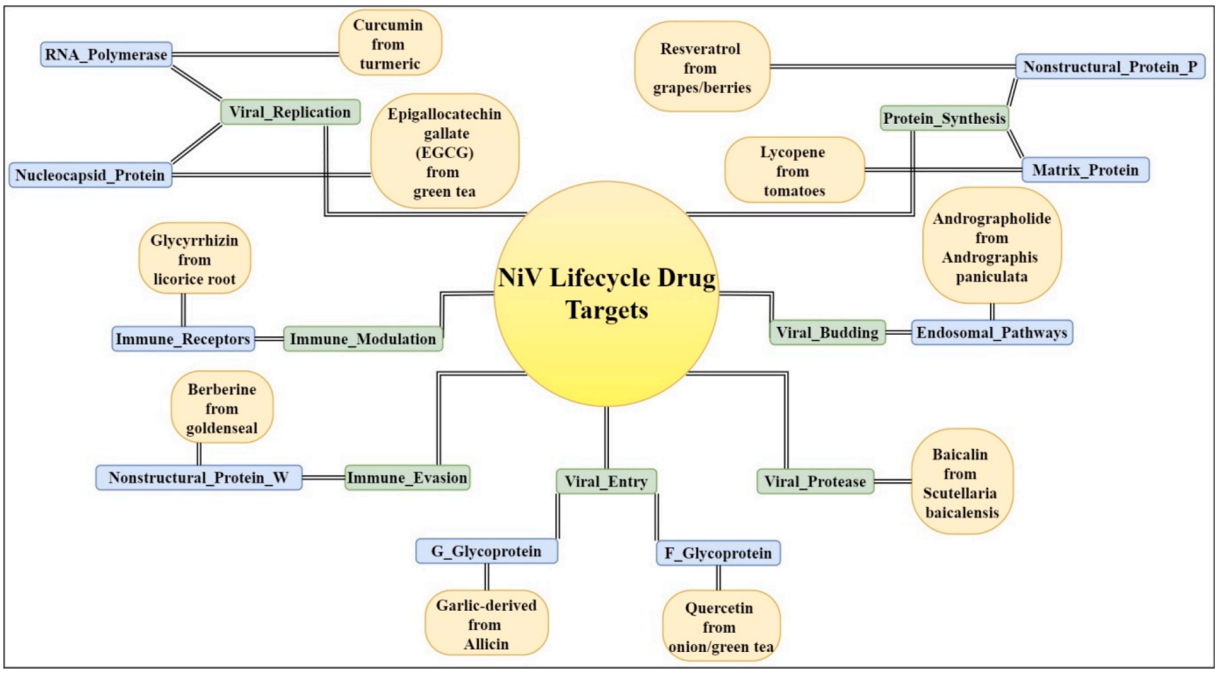

Fig. 1. Natural compounds targeting key stages in the Nipah virus lifecycle, including viral entry, replication, protein synthesis, and immune evasion.

3. Methods

3.1. Database of FDA-approved drugs

The procedure for gathering a comprehensive collection of FDA approved drugs for potential repurposing against NiV involves consulting a dependable drug database or library, such as Drug Bank, PubChem, and WHO. Following this, we have compiled a comprehensive collection of FDA-approved pharmaceutical drugs across several therapeutic categories in our in-house library, and the library consists of 4344 drugs, which can be utilized to investigate repurposing active drugs.

3.2. Network pharmacology

The implementation of graph theoretical analysis was facilitated by utilizing the Kyoto Encyclopedia of Genes and Genomes database. This study chose the homo sapiens protein interaction network (hsa04360) as the fundamental framework for selecting the proteins with the highest degree of effect.

3.3. Molecular docking

The study focused on applying AutoDock Vina Version 1.2.0 by POAP script for in-silico modelling of developed molecules [18,19]. The Ephrin-B2 protein X-ray crystal structure (PDB: 2VSM) was obtained from the Research Collaboratory for Structural Bioinformatics (RCSB) Protein Data Bank.

3.4. Molecular dynamics simulation

Molecular dynamics simulation studies were performed on the protein 2VSM, with Guamecycline, Ergotamine, Sancycline, Entrectinib and Atogepant as the active constituent. The simulations were conducted utilizing the Desmond software, which D. E. Shaw Research developed [18,19]. The protein was submerged in a solvent model called TIP3P, which comprised water molecules organized in a three-centred arrangement. The solvation procedure was conducted within a cubic container. The protein atoms were situated at a distance of 10 Å and angles of 90.0 relative to the periphery of the simulation box, creating a buffer zone between them. The process of neutralizing a system was accomplished by adding sodium ions with a concentration. The dynamics of the protein–ligand complex were simulated for 100, 500 and 1000 ns and the visual analysis of trajectories and 3D structures was conducted utilizing the Maestro graphical interface after the simulation.

4. Results and discussion

4.1. Network pharmacology

The route was graphically represented using the hsa04360 dataset, with proteins as nodes and interactions as edges [20,21]. This representation may be observed in Fig. 2. The network consisted of 141 nodes and 192 edges. The relevance of proteins was determined by evaluating the parameters' values. Based on the average measurement of each parameter, a set of highly significant proteins can be identified. These proteins include **Ephrin-B2** EPHB1 PLXNB2 PLXNA1 ROBO1 ROBO2 DCC NGEF DPYSL2 CDC42 RAC1 RHOA ABL1 EPHA2 NTN1 NRP1 PTCH1 BMPR2 WNT5A TRPC1 FYN DCC NEO1 PARD3 GNAI1 CXCR4 DCC PPP3CA ITGB1 RASA1 CXCR4 LRRC4C EFNA1 RHOA SRGAP2 LRRC4 SMO PRKCA FYN FZD3 RAC1 RND1 PRKCZ ABL1 NCK2 BOC PAK4 PTK2 SRC PTK2. Within the top 141 nodes, the observed outcomes for Ephrin-B2 were as follows: a Stress centrality score of 16752, a Radiality centrality score of 6.3, an Eigenvector centrality score of 0.562684, an Eccentricity centrality score of 0.142857, a Closeness centrality score of 0.004065, a Betweenness centrality score of 6001.776, and a degree centrality score of 34 within the network. Identifying the pharmacological target Ephrin-B2 for NiV therapy was based on significant metrics, as indicated by the threshold values presented in Table 1. Ephrin-B2 garners greater attention due to its involvement in the interaction with NiV proteins, which is a significant factor contributing to the propagation of the disease. The selection of Ephrin-B2 as a significant target in network pharmacology was based on the analytical report of graph theory and its associated relevance.

4.2. Mechanism of Ephrin-B2

Ephrin-B2 (EFNB2) assumes a pivotal function in the infection mechanism of the Nipah virus (NiV) by acting as a cellular receptor

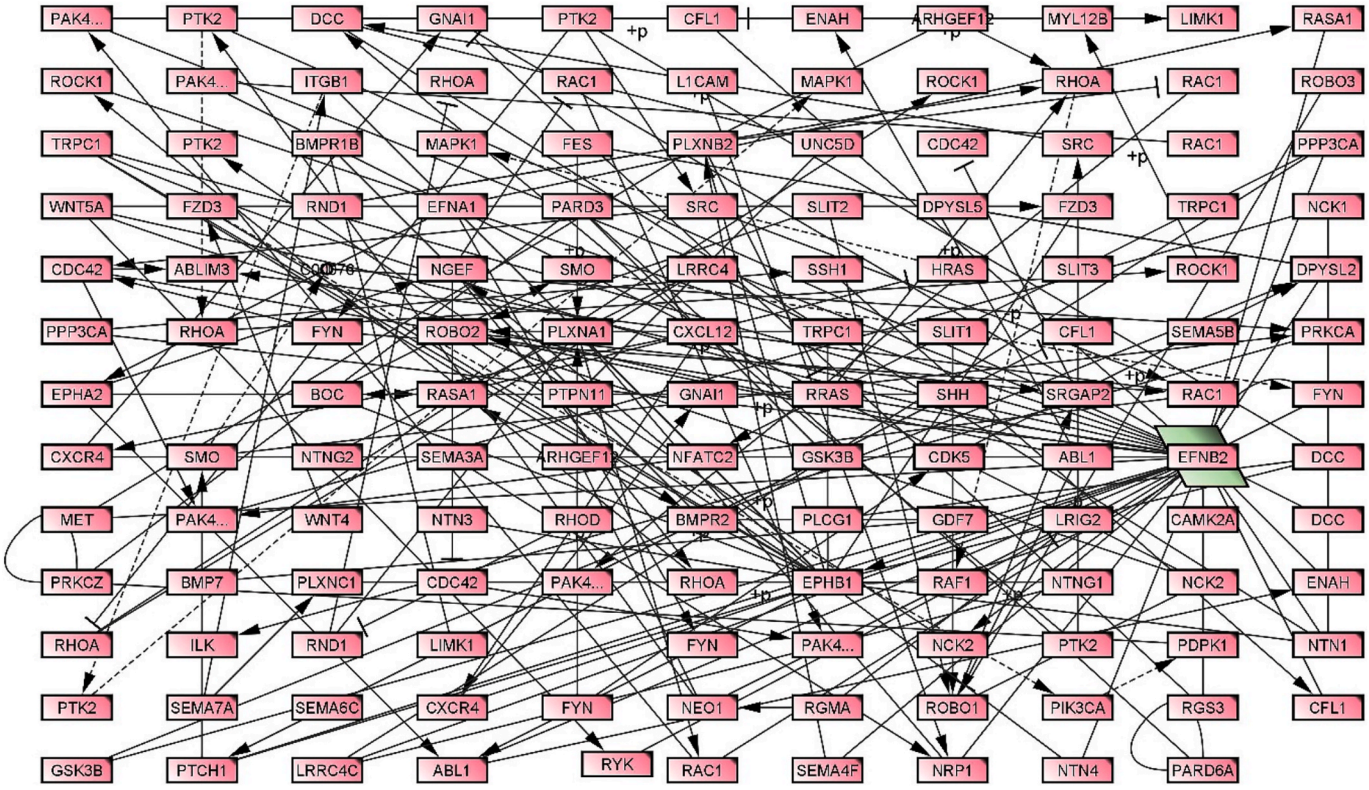

Fig. 2. Graphical representation of Nodes and Edges of EFNB2 Network.

employed by the virus to enter host cells [1]. The underlying process by which ephrin-B2 contributes to NiV infection can be succinctly stated as follows: The first stage of Nipah virus (NiV) infection entails the interaction between the attachment glycoprotein (NiV-G) located on the viral envelope and ephrin-B2 present on the host cell's surface. Ephrin-B2 is a receptor for the glycoprotein G of Nipah virus (NiV). The aforementioned binding event is particular and crucial for the virus's capacity to infiltrate host cells. Upon binding to ephrin-B2, NiV-G initiates a cascade of conformational alterations within the virus, facilitating its fusion with the cellular membrane of the host. This fusion event facilitates the entry of the viral genetic material (RNA) into the host cell's cytoplasm. Upon entering the host cell, the NiV proceeds to undergo replication of its RNA genome and subsequently generates novel viral particles. Subsequently, these recently formed virions can disseminate and invade adjacent cells. It is crucial to acknowledge that the association between ephrin-B2 and NiV-G exhibits a remarkable level of specificity, which significantly influences the range of hosts and the preference for specific tissues by the NiV. Ephrin-B2 exhibits expression in diverse tissue types, encompassing the neurological system and endothelial cells, both serving as specific targets for the NiV. One of the factors contributing to the heightened pathogenicity of the NiV is its unique characteristics. The comprehension of the involvement of ephrin-B2 in NiV infection has played a pivotal function in advancing prospective therapeutic approaches and interventions aimed at impeding the virus's entry into host cells Fig. 3.

4.3. Details about protein 2VSM

In the research paper by [22], the investigation focused on applying Homo Sapiens, Hydrolase, and X-Ray Diffraction techniques to address the structural elucidation of the 550-residue protein 2VSM. Through their efforts, the researchers successfully identified a total of 5272 atoms present inside the protein. Additionally, they made significant progress in their investigation of the cell line Hek293t, showing remarkable efficacy as a potent and specific inhibitor of NiV. The authors determined the resolution of the protein structure to be 1.80 Angstroms and identified two distinct chains, labelled as chain A and chain B. Chain A contains a Hemagglutinin-Neuraminidase molecule characterized by a B-Propeller structure, an Ephrin Binding Domain, and Residues 188. On the other hand, Chain B consists of Ephrin-B2, which possesses a Receptor-Binding Domain spanning Residues 28–165. The laboratory can efficiently generate the proteins at a scale suitable for conducting clinical trials, and the outcomes obtained thus far exhibit promising prospects.

4.4. Molecular docking studies

The study involved collecting 4,344 ligands sourced from the FDA-approved pharmaceuticals database. These ligands underwent molecular docking examinations against the Ephrin-B2 protein (PDB: 2VSM). The drugs with the highest recorded scores are derived from an internal database consisting of drugs approved by the FDA that are Guamecycline with a binding energy of −13.3 kcal × mol^{-1}, Ergotamine with a binding energy of −12.2 kcal × mol^{-1}, Sancycline with a binding energy of −9.6 kcal × mol^{-1}, Entrectinib with a binding energy of −12.1 kcal × mol^{-1}, Atogepant with a binding energy of −12.0 kcal × mol^{-1}, Etoposide with a binding energy of −11.8 kcal × mol^{-1}, Venetoclax with a binding energy of −11.8 kcal × mol^{-1}, Lumacaftor with a binding energy of −11.7 kcal × mol^{-1}, Ubrogepant with a binding energy of −11.7 kcal × mol^{-1}, Eltrombopag with a binding energy of −11.6 kcal × mol^{-1}, Fosnetupitant with a binding energy of −11.6 kcal × mol^{-1}, Lomitapide with a binding energy of −11.6 kcal × mol^{-1}, Lifitegrast with a binding energy of −11.5 kcal × mol^{-1}, Azilsartan_Medoxomil with a binding energy of −11.4 kcal × mol^{-1}, Baloxavir_Marboxil with a binding energy of −11.4 kcal × mol^{-1}, Grapiprant with a binding energy of −11.4 kcal × mol^{-1}, Metacycline with a binding energy of −11.4 kcal × mol^{-1}, Midostaurin with a binding energy of −11.4 kcal × mol^{-1}, Olaparib with a binding energy of −11.4 kcal × mol^{-1}, Tucatinib with a binding energy of −11.4 kcal × mol^{-1}, Irinotecan with a binding energy

Table 1
The results of network analysis with receptors threshold parameter values.

Label	Degree	Betweenness	Closeness	Eccentricity	EigenVector	Radiality	Stress
EFNB2	34	6001.776	0.004065	0.142857	0.562684	6.3	16,752
EPHB1	24	8448.236	0.004464	0.166667	0.411307	6.457143	21,392
PLXNB2	7	1252.685	0.003322	0.142857	0.104016	5.907143	6070
PLXNA1	7	1661.684	0.003356	0.142857	0.095791	5.928571	3902
ROBO1	6	247.5449	0.00207	0.111111	0.009948	4.607143	1680
ROBO2	6	1841.619	0.003289	0.142857	0.072436	5.885714	6104
DCC	5	463.3023	0.003185	0.142857	0.100079	5.9	1928
NGEF	5	535.8725	0.003195	0.142857	0.07853	5.821429	2082
DPYSL2	5	493.2395	0.003135	0.125	0.111936	5.778571	980
CDC42	5	781.3859	0.003058	0.125	0.097495	5.807143	3420
RAC1	4	14.73774	0.002004	0.1	0.011691	4.578571	60
RHOA	4	230.014	0.002049	0.111111	0.008	4.657143	1596
ABL1	4	209.7295	0.003559	0.142857	0.173715	6.135714	808
EPHA2	4	175.1353	0.002681	0.125	0.052905	5.392857	1030
NTN1	4	853.1327	0.00361	0.142857	0.172289	6.078571	1868
NRP1	4	675	0.002564	0.125	0.015702	5.271429	1302
PTCH1	4	969.1701	0.003663	0.142857	0.157746	6.107143	1688
BMPR2	4	1029.223	0.003247	0.142857	0.091881	5.857143	2242
WNT5A	4	27.28658	0.002994	0.125	0.113741	5.671429	98
TRPC1	4	195.2815	0.003497	0.142857	0.162534	6.1	600
FYN	4	176.9797	0.002421	0.111111	0.02067	5.192857	966
DCC	4	714.1517	0.00271	0.125	0.028516	5.507143	1384
NEO1	4	602.9796	0.002392	0.111111	0.014925	5.071429	1198
PARD3	3	384.0197	0.001527	0.1	4.80E-05	3.378571	706
GNAI1	3	1.833333	0.002994	0.125	0.118089	5.757143	4
CXCR4	3	294.228	0.003185	0.142857	0.068411	5.9	566
DCC	3	66.47707	0.003012	0.125	0.127337	5.771429	280
PPP3CA	3	227.5	0.003067	0.125	0.105665	5.814286	400
ITGB1	3	387.7984	0.003215	0.142857	0.067424	5.835714	1050
RASA1	3	477.8942	0.003279	0.142857	0.072514	5.964286	1198
CXCR4	3	91.375	0.003003	0.125	0.107911	5.764286	146
LRRC4C	3	35.07958	0.002994	0.125	0.114134	5.671429	98
EFNA1	3	153.9736	0.002398	0.111111	0.022183	5.078571	872
RHOA	3	160.7258	0.002217	0.111111	0.004916	4.921429	410
SRGAP2	3	223.966	0.002551	0.125	0.012862	5.257143	992
LRRC4	3	370.1158	0.002463	0.125	0.010817	5.157143	752
SMO	3	671.25	0.00271	0.125	0.025472	5.507143	1026
PRKCA	3	227	0.002179	0.111111	0.004695	4.778571	346
FYN	3	61.41667	0.003049	0.125	0.089556	5.714286	138
FZD3	3	1457.52	0.003257	0.166667	0.065819	5.95	2406
RAC1	3	249.5406	0.003125	0.125	0.116918	5.857143	812
PAK4	3	121.9463	0.00303	0.125	0.108252	5.785714	380
RND1	3	112.8182	0.002604	0.125	0.017656	5.4	436
PRKCZ	3	602.5197	0.001779	0.111111	2.99E-04	4.042857	1050
ABL1	3	236.4254	0.002525	0.125	0.012862	5.314286	992
NCK2	3	308.0747	0.002551	0.125	0.012869	5.342857	1336
BOC	3	168.8299	0.003125	0.142857	0.07181	5.771429	420
PTK2	3	102.6009	0.002506	0.125	0.021451	5.292857	676
SRC	3	55.28433	0.002381	0.111111	0.019921	5.142857	616
PTK2	3	1281.727	0.00303	0.125	0.090229	5.785714	2754

of −11.4 kcal × mol^{-1}, Oxytetracycline with a binding energy of −11.4 kcal × mol^{-1}, Tepotinib with a binding energy of −11.3 kcal × mol^{-1}, Afoxolaner with a binding energy of −11.2 kcal × mol^{-1}, Eltrombopag with a binding energy of −11.2 kcal × mol^{-1}, Posaconazole with a binding energy of −11.2 kcal × mol^{-1}, and Ruboxistaurin with a binding energy of −11.2 kcal × mol^{-1} towards the Ephrin-B2 protein. The amino acids exhibited the most significant interaction with Guamecycline, Ergotamine, Sancycline, Entrectinib and Atogepant. The amino acid residues involved in the interaction of Guamecycline were GLU 579, LYS 560, VAL 507, ASP 302, HIS 281, SER 245, GLY 243, SER 241, ARG 236, PRO 220, and SER 121. The amino acid residues involved in the interaction of Ergotamine were LYS 560, ARG 242, and LEU 124. The amino acid residues involved in the interaction of Sancycline were LYS 560, VAL 507, ASP 302, CYS 240, and ARG 236. The amino acid residues involved in the interaction of Entrectinib were GLU.

579, LYS 560, VAL 507, GLN 559, ASP 302, HIS 281, TYR 280, ASP 219, GLY 126, and SER 121. The amino acid residues involved in the interaction of Atogepant were LYS 560, GLN 559, LEU 305, ASP 302, TYR 351, HIS 281, SER 245, LEU 124 ASN 123, and SER 121. The observed findings suggest that the active constituents Guamecycline, Ergotamine, Sancycline, Entrectinib and Atogepant exhibit significant inhibition of the Ephrin-B2 protein. Consequently, these results indicate a promising potential for the treatment of NiV. The binding interactions, 2D and 3D models of active drugs Guamecycline, Ergotamine, Sancycline, Entrectinib and Atogepant were shown in Table 2, Fig. 4.

4.5. Molecular dynamic studies

Computations were conducted to ascertain the protein–ligand complex's root-mean-square deviation (RMSD) and root-mean-square fluctuation (RMSF). Furthermore, an investigation was conducted to analyze and elucidate the interaction patterns exhibited by the protein–ligand complex about the FDA-approved drugs Guamecycline, Ergotamine, Sancycline, Entrectinib, and Atogepant. The significant impact of protein–ligand contacts and interaction fingerprints on the complex was determined by analyzing the interactions with amino acid residues and calculating the RMSD and RMSF. Fig. 5 depict the protein–ligand and molecular interactions of Guamecycline, Ergotamine,

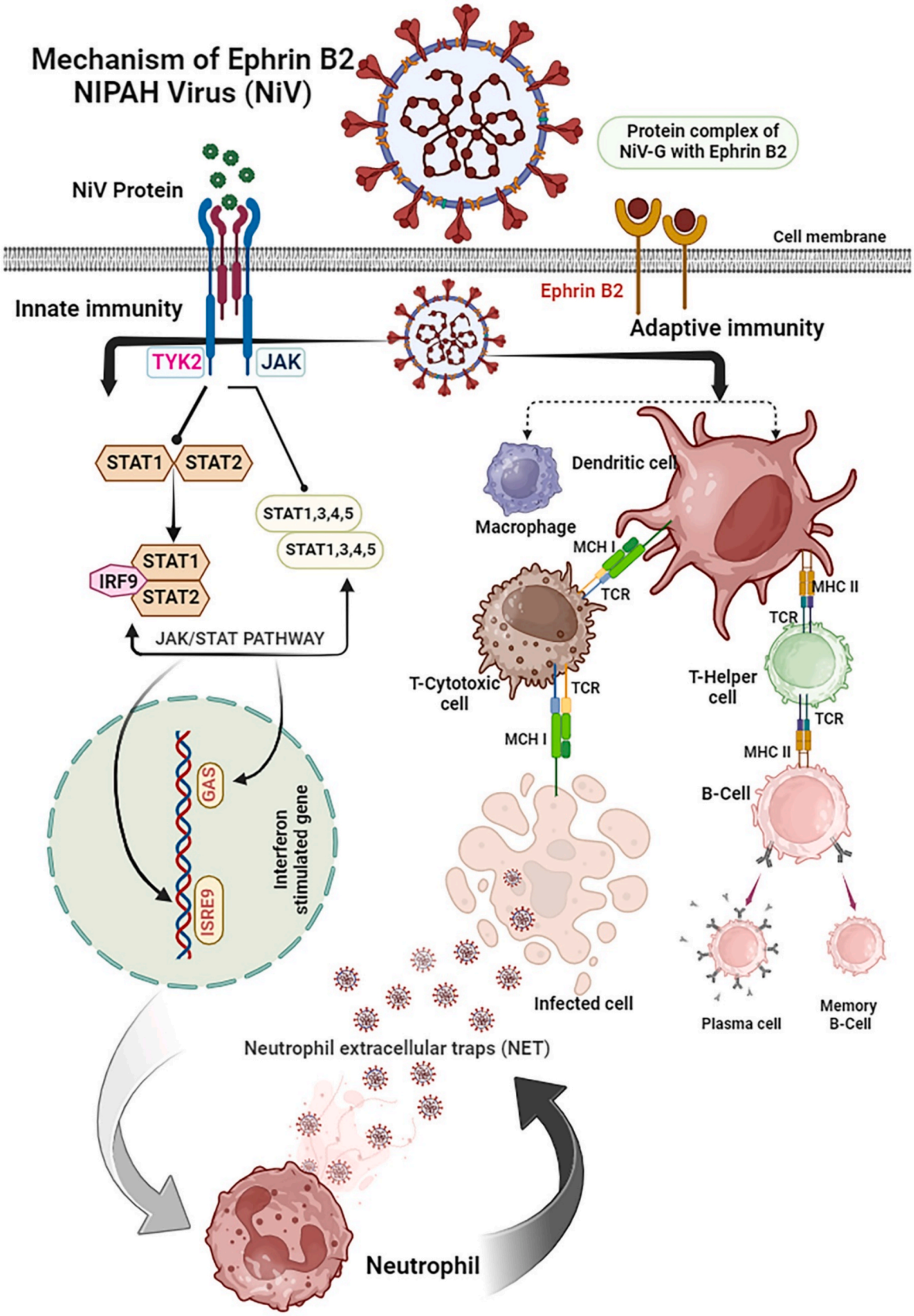

Fig. 3. Mechanism of action of EFNB.

Table 2
The best compounds and its energy values.

Ligand Name	Score
Guamecycline	−13.3
Ergotamine	−12.2
Sancycline	−12.2
Entrectinib	−12.1
Atogepant	−12
Etoposide	−11.8
Venetoclax	−11.8
Lumacaftor	−11.7
Ubrogepant	−11.7
Eltrombopag_1	−11.6
Fosnetupitant	−11.6
Lomitapide	−11.6
Lifitegrast	−11.5
Azilsartan_Medoxomil	−11.4
Baloxavir_Marboxil	−11.4
Grapiprant	−11.4
Metacycline	−11.4
Midostaurin	−11.4
Olaparib	−11.4
Tucatinib	−11.4
Irinotecan	−11.3
Oxytetracycline	−11.3
Tepotinib	−11.3
Afoxolaner	−11.2
Eltrombopag	−11.2
Posaconazole	−11.2
Ruboxistaurin	−11.2
ZINC000100303296	**−9.8**
ZINC000257351316	**−13.4**
ZINC000169368545	**−11.8**
ZINC000004879678	**−9.8**
ZINC000059697693	**−10.9**

Sancycline, Entrectinib, and Atogepant. The Guamecycline molecule exhibited a range of interatomic distances between 3.52Å and 2.38 Å. Notably, during the molecular dynamics (MD) simulation, the Protein-Ligand Contacts exhibited strong interactions between Guamecycline and active amino acids, namely GLU 579 (with a 77 % relationship), ASP 302 (with a 95 % relationship), and ARG 236. During the MD simulation, the interaction of ergotamine was observed within a range of 2.27 to 1.09 Å. Specifically, the amino acids HIS 281 exhibited a 52 % interaction, ASP 302 showed a 47 % interaction, and ARG 236 also displayed an interaction. During the MD simulation, the Sancycline molecule exhibited a range of distances between 1.82 and 4.11 Å. Furthermore, the amino acids SER 121 and GLU 119 had significant interactions with Sancycline, with 35 % and 32 % interaction percentages, respectively. The MD simulation showed that Entrectinib maintained interactions with amino acids LYS 560 (42 % interaction), ASN 306 (47 % interaction), and SER 121 (75 % interaction) within a range of 2.27 to 1.09 Å. The MD simulation depicted the retention of Atogepant within a region of 1.59 to 8.15 Å, together with the amino acids ARG 236 (with a 70 % interaction), LEU 124 (with a 77 % interaction), and GLU 97 (with a 47 % interaction). The RMSD complex and protein–ligand contacts provide compelling evidence of the involvement of specific amino acids, namely GLU 579, LYS 560, VAL 507, ASP 302, HIS 281, SER 245, GLY 243, SER 241, ARG 236, PRO 220, and SER 121, in the interaction for Guamecycline. These interactions were retained throughout the simulation, as depicted in Fig. 6.

The stability of the Ephrin-B2 Protein-ligand complexes, specifically the ligands Guamecycline, Ergotamine, Sancycline, Entrectinib, and Atogepant, was assessed by measuring the Prot_CA (Protein C-alpha) and Lig_wrt_Protein (Ligand concerning Protein) values acquired over a 100 ns molecular dynamics production run. The EFNB2-ligand complexes of Guamecycline exhibited average Prot_CA, and

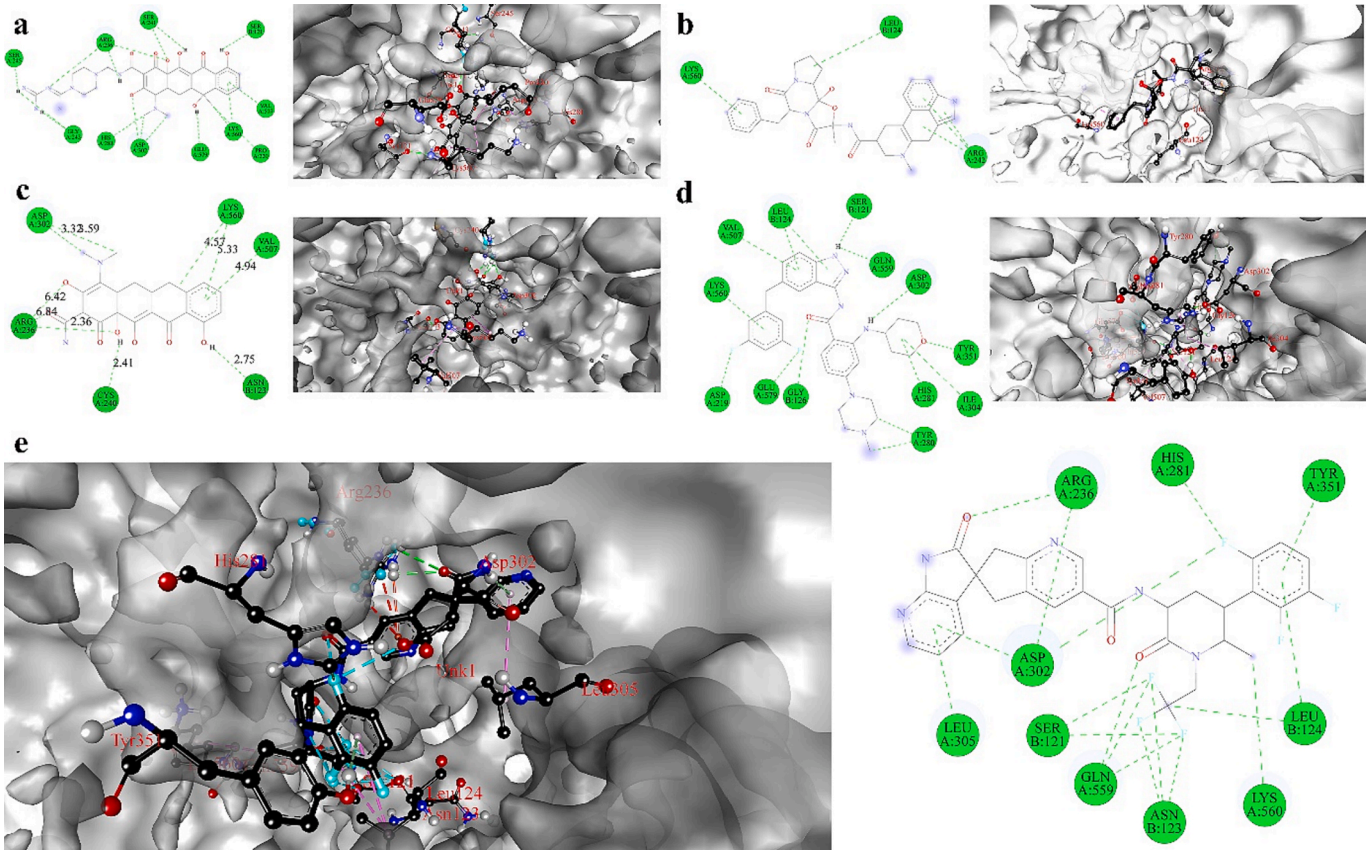

Fig. 4. The graphical representation of 2D, 3D and amino acid interactions of a) EFNB2-Guamecycline complex, b) EFNB2-Ergotamine complex, c) EFNB2-Sancycline complex, d) EFNB2-Entrectinib complex, and e) EFNB2-Atogepant complex.

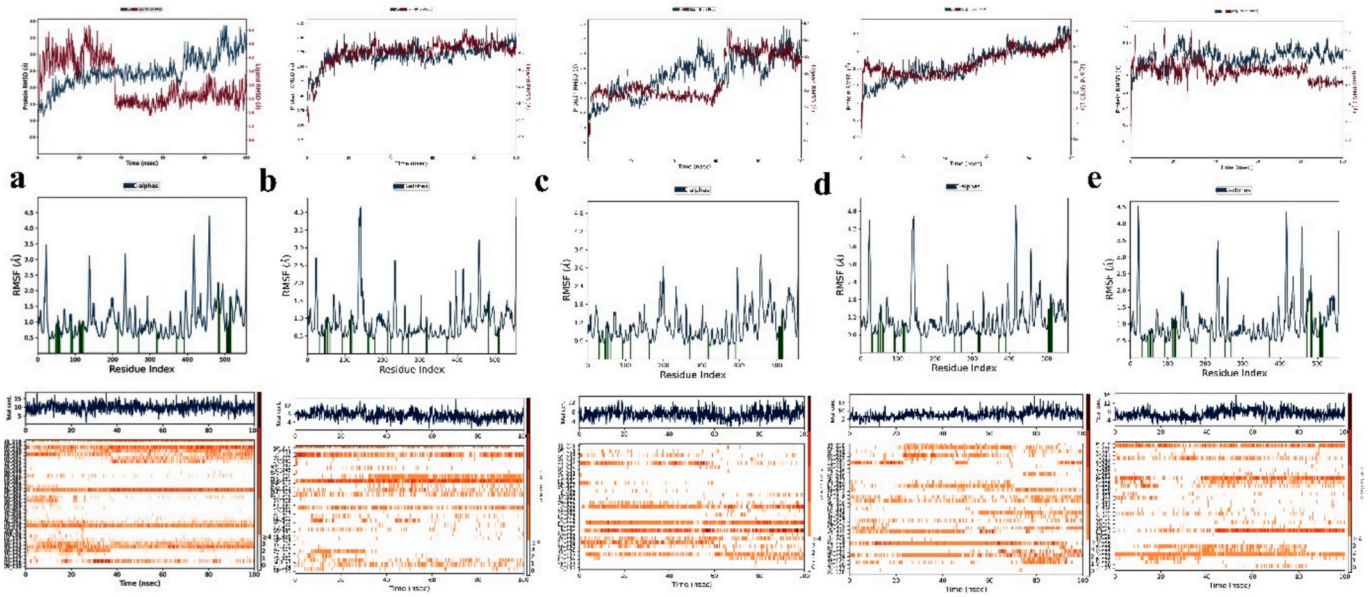

Fig. 5. The RMSD, RMSF and protein–ligand contacts of a) EFNB2-Guamecycline complex, b) EFNB2-Ergotamine complex, c) EFNB2-Sancycline complex, d) EFNB2-Entrectinib complex, and e) EFNB2-Atogepant complex in 100 ns.

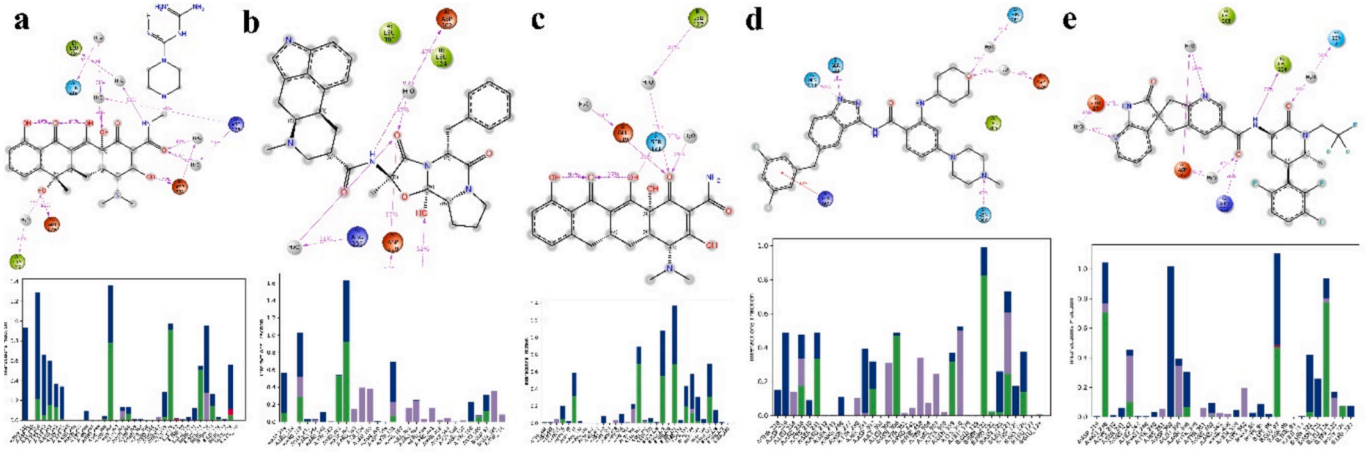

Fig. 6. The protein–ligand contacts and amino acid interaction fraction of a) EFNB2-Guamecycline complex, b) EFNB2-Ergotamine complex, c) EFNB2-Sancycline complex, d) EFNB2-Entrectinib complex, and e) EFNB2-Atogepant complex.

Lig_with_Protein, values of 2.485499 ns (ns), and 3.071333 ns, respectively. In contrast, the Ergotamine complex had a Prot_CA value of 1.700236 ns and a Lig_wrt_Protein value of 4.818807. The Sancycline complex exhibited a Prot_CA value of 2.226909 ns and a Lig_wrt_Protein value of 3.7469 ns. Similarly, the Entrectinib complex displayed a Prot_CA value of 2.115415 ns and a Lig_wrt_Protein value of 3.576862 ns. Lastly, the Atogepant complex exhibited a Prot_CA value of 1.835033 ns and a Lig_wrt_Protein value of 3.856856. Notably, the Guamecycline complex exhibits more excellent stability than Ergotamine, Sancycline, Entrectinib, and Atogepant complexes. The observed significant RMSD result of Guamecycline in 100 ns prompted us to increase its molecular dynamics production run up to 1000 ns. The EFNB2-Guamecycline complex Prot_CA value was 2.218879 ns, and the Lig_wrt_Protein value was found to be 2.303156 ns in 1000 ns root mean square deviation RMSD trajectories. The data obtained from the observation of the EFNB2-Guamecycline complex after 1000 ns provide clear evidence for the stability of Guamecycline Fig. 7.

The RMSF values of protein–ligand complexes of Guamecycline, Ergotamine, Sancycline, Entrectinib, and Atogepant exhibited no fluctuations throughout the molecular dynamic's simulation. It was observed that the fluctuation curve of Guamecycline exhibited a lower magnitude compared to the fluctuation curves of Ergotamine, Sancycline, Entrectinib, and Atogepant complexes. The RMSF curves associated with Guamecycline generally exhibited no fluctuation and excellent stability compared to the other compounds. This observation suggests that Guamecycline has the propensity to form more stable complexes with Ephrin-B2.

The torsional conformations of the rotatable bonds in the ligand were computed during the simulation trajectory to gain insight into the conformational changes shown by the detected ligands. The dartboard plots on the left visually represent the angular orientation of each bond at specific time points throughout the simulations. The initial placement of the simulations was cantered within the radial plot, and the temporal progression was represented by outward radial plotting. The histograms on the right-hand side illustrate the probability distribution of torsions concerning the angle. In this representation, the radial coordinate represents the torsion potential of the rotatable bond, while the angular coordinate corresponds to the torsional angle. The Guamecycline

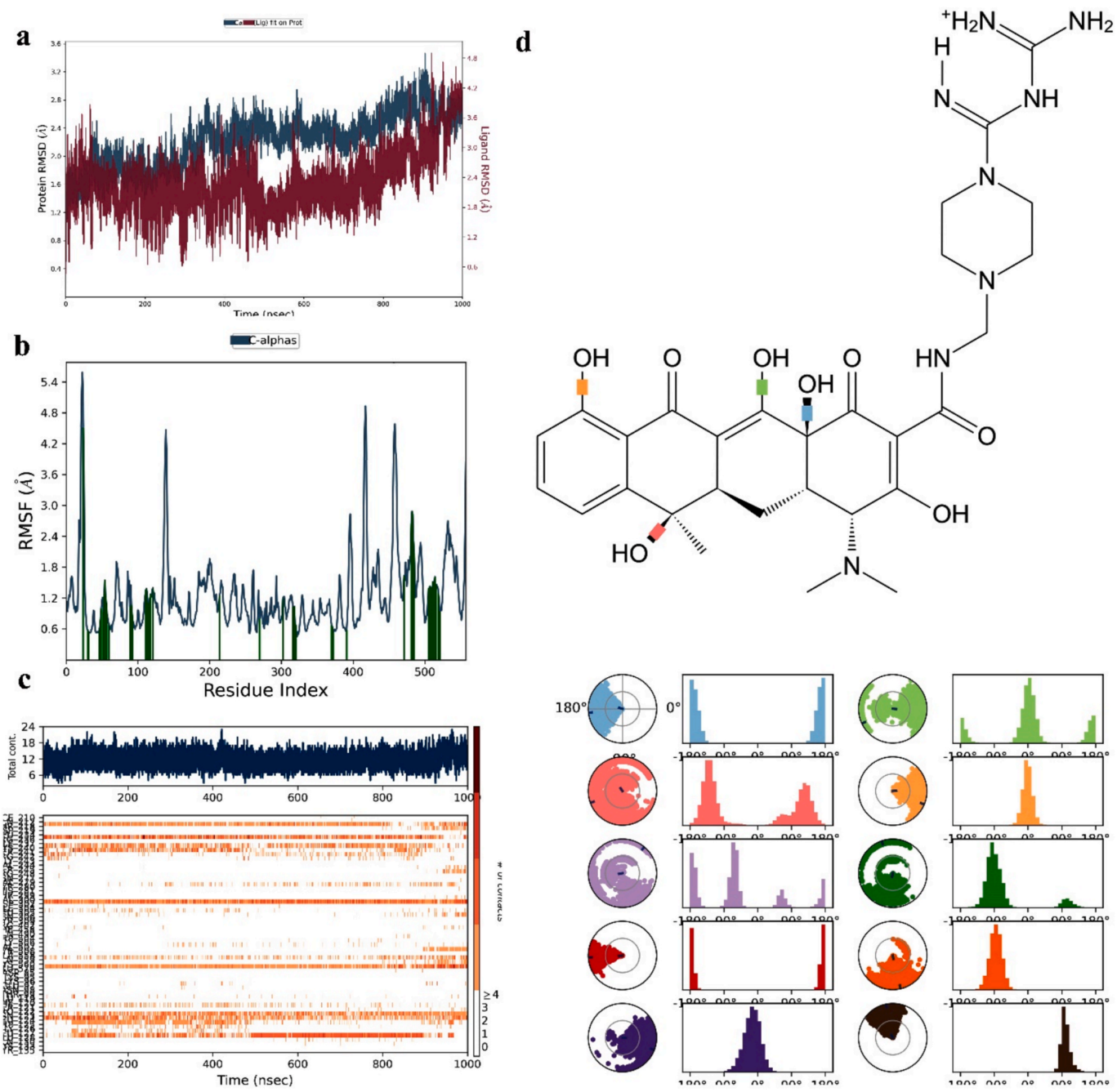

Fig. 7. The a) RMSD, b) RMSF, c) protein–ligand contacts, and d) torsional conformation of each rotatable bond, angle of the EFNB2- Guamecycline complex in 1000 ns.

structure exhibits a tight connection between the tetrahydro tetracenedione and piperazine-1-carboximidamide moieties through hydrogen bonding Fig. 7. The dial plots and bar charts presented in the study indicate that Guamecycline had higher levels of rigidity, greater flexibility Fig. 7. Based on the results obtained from the MD simulation, it was observed that Guamecycline exhibited substantial interaction with the Ephrin-B2 protein (PDB: 2VSM). Consequently, Guamecycline exhibits promise as a viable lead compound for the therapeutic intervention of NiV.

4.6. Molecular docking and dynamic study of similar structures of Guamecycline

To obtain sub-structures of Guamecycline, we have used the Zinc Database online at the following web address: https://cartblanche22.docking.org/. Utilize the sub-structure search tool available on the Zinc Database website to locate compounds that have structural similarities to Guamecycline. Use the SMILES notation of Guamecycline in the "Search" or "Substructure Search" option; click the "Search" button to get the process started in the Zinc Database that presents a list of compounds that have a substructure that is comparable to that of the Guamecycline. The results showed that five similar structures include the compound's 2D and 3D structures, chemical properties, and other structural information. Further, the SDF format of their structures was downloaded for molecular modelling investigation. The study involved the utilization of a collection of 5 similar structures of Guamecycline ZINC IDs ZINC000100303296, ZINC000257351316, ZINC000169368545, ZINC000004879678, and ZINC000059697693

sourced from the Zinc substructure database. These ligands underwent molecular docking examinations against the Ephrin-B2 protein (PDB: 2VSM). The drugs with the highest recorded scores are derived from an internal database of similar Guamecycline structures. ZINC000257351316 with a binding energy of −13.4 kcal × mol^{-1}, Compound 3 with a binding energy of −11.8 kcal × mol^{-1}, Compound 5 with a binding energy of −10.9 kcal × mol^{-1}, Compound 1 with a binding energy of −9.8 kcal × mol^{-1}, Compound 4 with a binding energy of −9.8 kcal × mol^{-1}. The amino acids exhibited the most significant degree of interaction with ZINC000257351316. The amino acid residues involved in the interaction of ZINC000257351316 were ARG 242, ARG 236 and ASP 219 Table 2, Fig. 8.

The researchers performed calculations to determine the values of the RMSD and RMSF for the protein–ligand combination of Guamecycline and structurally similar ZINC000257351316. Moreover, a comprehensive examination was undertaken to investigate and clarify the interaction patterns of Guamecycline and structurally similar ZINC000257351316. The MD simulation was run on 500 ns, and ZINC000257351316 showed that the maintained interactions of amino acids CYS 282 (74 %), PRO 220 (88 %), ASP 219 (87 %), and TRP 125 (62 %) within a range of 2.40 to 2.08 Å. Furthermore, the EFNB2-structurally similar ZINC000257351316 complex average value of Prot_CA was 2.254743 ns, and the Lig_wrt_Protein value was found to be 3.092464 ns in 500 ns RMSD trajectories. The data obtained from the observation of the EFNB2- structurally similar ZINC000257351316 complex after a duration of 500 ns provide clear evidence for the stability of structurally similar ZINC000257351316 Fig. 9. The ZINC000257351316 data revealed no fluctuations observed in the RMSF values with the duration of 500 residue index.

The current study was evident for drug repurposing because the observed results indicate that the interaction of amino acids, namely **GLU 579, LYS 560, VAL 507, ASP 302, HIS 281, SER 245, GLY 243, SER 241, ARG 236, PRO 220,** and **SER 121** was retained **in** docking, 1000 ns of Guamecycline dynamic simulation and 500 ns of Guamecycline structurally similar ZINC000257351316 dynamic simulation Fig. 10. In addition to the retention of amino acids, better stability was observed in RMSD, and no fluctuations were observed in RMSF throughout the dynamic simulation. Based on the report it was expected that Guamecycline is being evaluated alongside established NiV inhibitors such as remdesivir and favipiravir, as well as repurposed medicines like ribavirin. Unlike the other options, Guamecycline demonstrates exceptional effectiveness in specifically targeting the glycoproteins and polymerase of NiV, providing a distinct and unique method of action. The safety characteristics and the development of resistance of the subject also vary, which justifies the need for additional research. Guamecycline's mechanism of action is expected to involved a more effectively to inhibit the Ephrin-B2 target. The utilization of FDA-approved drugs to treat NiV presents a potentially fruitful approach in expediting the creation of therapeutic interventions to effectively counteract this very lethal infection, thereby addressing a pressing and unresolved medical requirement.

4.7. Limitations

The computational methodology employed for the discovery of drugs against the NiV encounters obstacles such as the possibility of imprecise docking scores and the dependability of molecular dynamics simulations. Although these approaches are potent, they may not comprehensively capture intricate biological interactions, resulting in less precise forecasts of medication effectiveness and stability, which requires additional experimental confirmation.

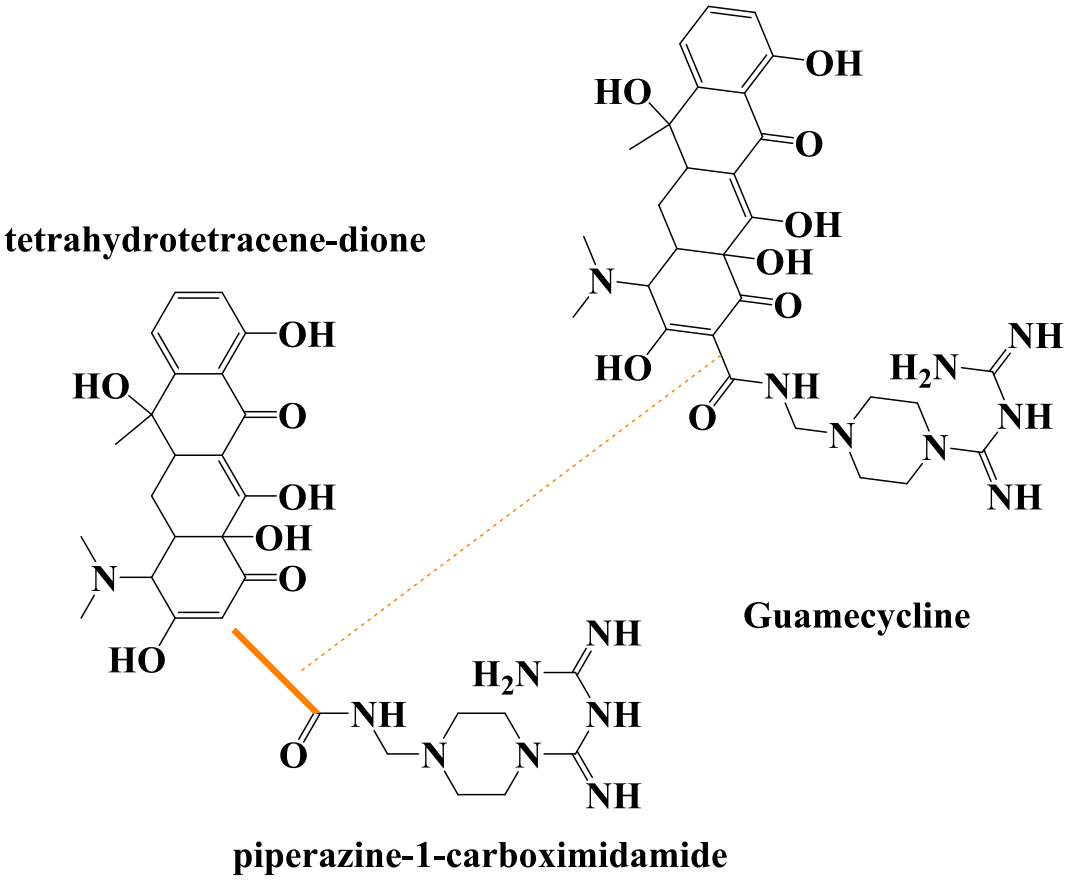

Fig. 8. A tight connection between the tetrahydrotetracene-dione and piperazine-1-carboximidamide in Guamecycline.

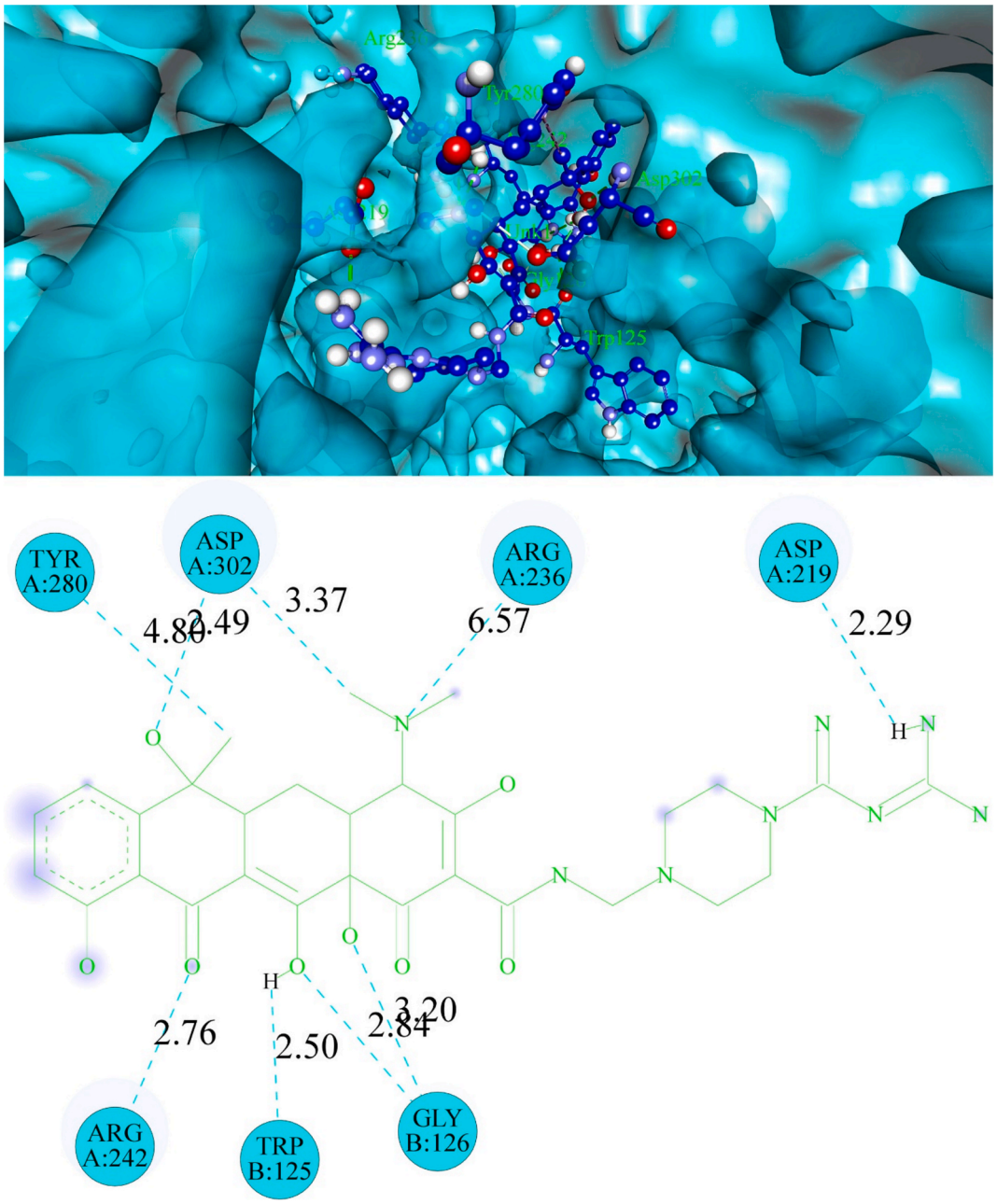

Fig. 9. The graphical representation of 2D, 3D and amino acid interactions of Structurally Similar EFNB2-ZINC000257351316 complex.

5. Conclusion

The present study employed a computational methodology to find pharmacological compounds derived from a database of 4344 drugs that have been approved by the FDA. Our analysis reveals that there are several FDA-approved medications that have favorable binding interactions with the Ephrin-B2 target. Within this FDA-approved medicine dataset, we have identified significant enhancements in the binding scores of various FDA-approved pharmaceuticals, such as Guamecycline, Ergotamine, Sancycline, Entrectinib, and Atogepant. Molecular dynamics simulations were used to evaluate the dynamic behavior of ligand–protein interactions, yielding valuable information about the stability and structural changes of drug-target complexes. This study proposes a simplified method for identifying the very potent lead chemical, Guamecycline. Furthermore, the sub-structures of Guamecycline were utilized to improve and confirm the stability of Guamecycline. More precisely, the sub-structure ZINC000169368545 was compared to Guamecycline, and the results showed that Guamecycline displayed superior features as a lead compound for inhibiting the target Ephrin-B2.

6. Authors' contributions

The project was conceived and managed by Dr. Panneerselvam Theivendren. The data analysis was conducted by Dr. Selvaraj Kunjiappan, Dr. Parasuraman Pavadai, Natarajan Kiruthiga, Anusuya M and Avinash D, the manuscript was authored by Dr. Panneerselvam Theivendren. The manuscript was reviewed by all authors.

CRediT authorship contribution statement

Panneerselvam Theivendren: Writing – review & editing, Writing – original draft, Software, Methodology, Conceptualization. **Selvaraj Kunjiappan:** Writing – review & editing, Writing – original draft,

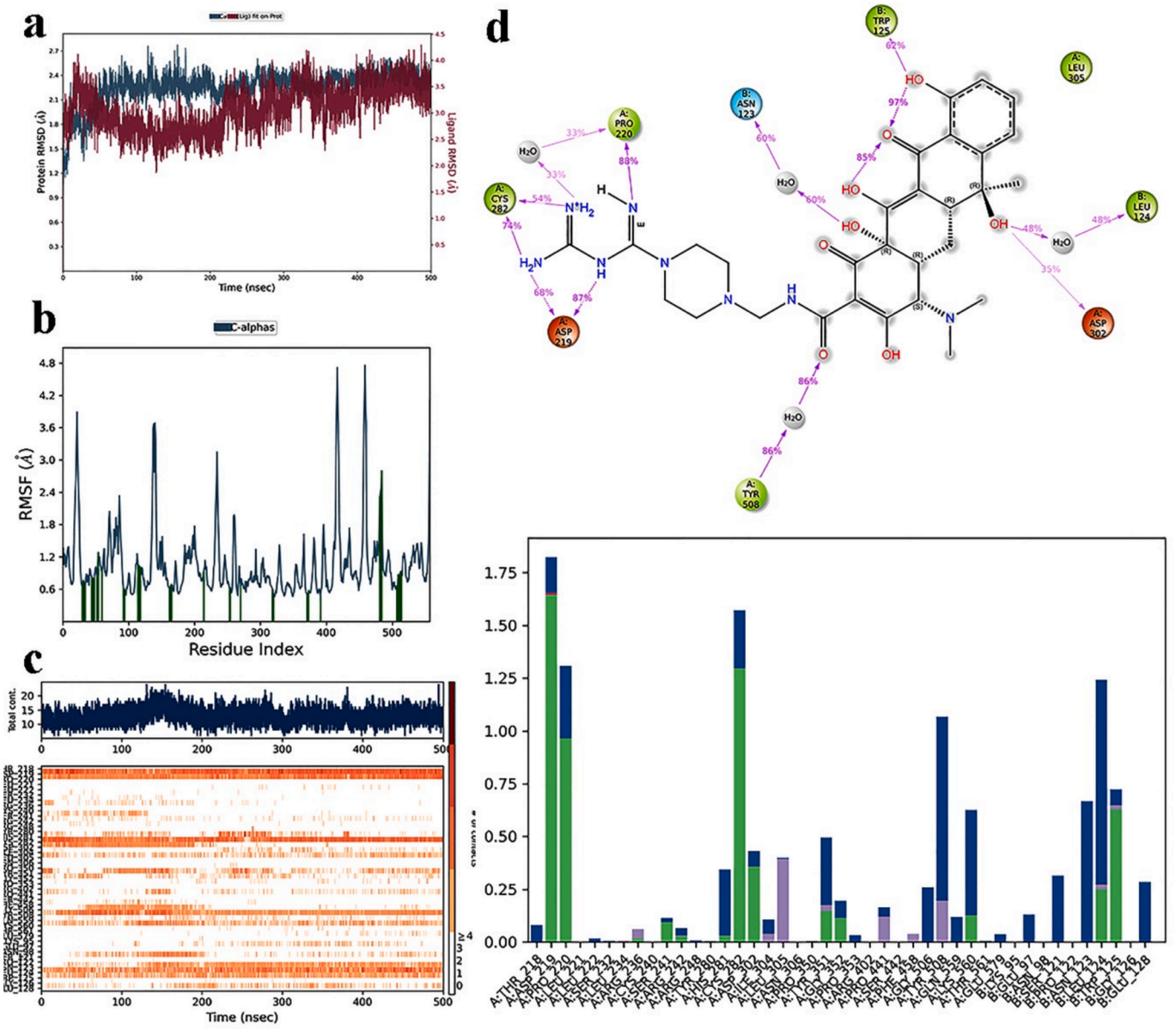

Fig. 10. The a) RMSD, b) RMSF, c) protein–ligand contacts, and d) amino acid interactions of the EFNB2- Structurally Similar ZINC000257351316 complex in 500 ns.

Methodology. **Parasuraman Pavadai:** Supervision, Software, Methodology. **Natarajan Kiruthiga:** Validation, Supervision, Investigation. **Anusuya Murugavel:** Validation, Investigation, Formal analysis. **Avinash Dayalan:** Validation, Supervision, Formal analysis.

Funding

This study was supported by the Vivekanandha Educational Institutions, Elayampalayam, Namakkal, Tamilnadu 637205, India and Department of Pharmaceutical Chemistry & Analysis, School of Pharmaceutical Sciences, Vels Institute of Science, Technology, & Advanced Studies, Pallavaram, Chennai, Tamil Nadu 600117, India [Seed grant number 110052023].

Declaration of competing interest

The authors declare that they have no known competing financial interests or personal relationships that could have appeared to influence the work reported in this paper.

Data availability

No data was used for the research described in the article.

References

[1] S. Yang, S. Kar, Comput. Biol. Med. 163 (2023) 107240.
[2] A. Mahfuz, M.A. Khan, E.H. Sajib, A. Deb, S. Mahmud, M. Hasan, O. Saha, A. Islam, M.M. Rahaman, Infect. Genet. Evol. 102 (2022) 105310.
[3] M.S. Kalbhor, S. Bhowmick, A.M. Alanazi, P.C. Patil, M.A. Islam, Biophys. Chem. 270 (2021) 106537.
[4] A. Rajput, A. Thakur, A. Rastogi, S. Choudhury, M. Kumar, Comput. Biol. Med. 136 (2021) 104677.
[5] B.A. Satterfield, B.E. Dawes, G.N. Milligan, Vaccine 34 (2016) 2971–2975.
[6] N. Thakur, D. Bailey, Microbes Infect. 21 (2019) 278–286.
[7] G. Arunkumar, S. Devadiga, A.K. McElroy, S. Prabhu, S. Sheik, J. Abdulmajeed, S. Robin, A. Sushama, A. Jayaram, S. Nittur, Clin. Infect. Dis. 69 (2019) 1752–1756.
[8] P. Majee, N. Jain, A. Kumar, J. Biomol. Struct. Dyn. 39 (2021) 1461–1480.
[9] S. Barua, A. Dénes, Heliyon (2023).

[10] E. de Wit, B.N. Williamson, F. Feldmann, K. Goldin, M.K. Lo, A. Okumura, J. Lovaglio, E. Bunyan, D.P. Porter, T. Cihlar, Antiviral Res. (2023) 105658.
[11] S. Ullah, R. Nawaz, S.A. AlQahtani, S. Li, A.M. Hassan, Results Phys. 51 (2023) 106629.
[12] D. Paul, A. Mohanty, A. Shah, B.K. Padhi, R. Sah, J. Biosafety Biosecur. 5 (2023) 57–59.
[13] S. Jain, M.K. Lo, M.H. Kainulainen, S.R. Welch, J.R. Spengler, S.M. Satter, M. Z. Rahman, M.E. Hossain, C.-F. Chiang, J.D. Klena, Virology 587 (2023) 109858.
[14] A. Berkane, N. Kundu, A.A. Munia, B. Chakrabarty, B.K. Utpal, N. Kumar, D. Vijay, M. Bourhia, Y.A.B. Jardan, G. Abdelkrim, J. Indian Chem. Soc. (2024) 101196.
[15] R.S. Jansi, A. Khusro, P. Agastian, A. Alfarhan, N.A. Al-Dhabi, M.V. Arasu, R. Rajagopal, D. Barcelo, A. Al-Tamimi, Sci. Total Environ. 759 (2021) 143539.
[16] A.-Q. Zhuang, Y. Chen, S.-M. Chen, W.-C. Liu, Y. Li, W.-J. Zhang, Y.-H. Wu, Viruses 15 (2023) 2315.
[17] D.R. Tompa, A. Immanuel, S. Srikanth, S. Kadhirvel, Int. J. Biol. Macromol. 172 (2021) 524–541.
[18] C. Palanichamy, P. Pavadai, T. Panneerselvam, S. Arunachalam, E. Babkiewicz, S. Ram Kumar Pandian, K. Shanmugampillai Jeyarajaguru, D. Nayak Ammunje, S. Kannan, J. Chandrasekaran, Molecules 27 (2022) 3799.
[19] A.K. Kalimuthu, T. Panneerselvam, P. Pavadai, S.R.K. Pandian, K. Sundar, S. Murugesan, D.N. Ammunje, S. Kumar, S. Arunachalam, S. Kunjiappan, Sci. Rep. 11 (2021) 21488.
[20] P.G. Dessai, S.P. Dessai, R. Dabholkar, P. Pednekar, S. Naik, S. Mamledesai, M. Gopal, P. Pavadai, B.K. Kumar, S. Murugesan, Mol. Divers. (2022) 1–20.
[21] P. Theivendren, S. Kunjiappan, S. Govindraj, J. Chandrasekarn, P. Pavadai, G. R. Saraswathy, I. Murugan, Drug Res. 69 (2019) 100–110.
[22] T.A. Bowden, A.R. Aricescu, R.J. Gilbert, J.M. Grimes, E.Y. Jones, D.I. Stuart, Nat. Struct. Mol. Biol. 15 (2008) 567–572.